Fundamental issues in nonlinear wide-band vibration energy harvesting

Einar Halvorsen*
Department of Micro and Nano Systems Technology, Faculty of Technology and Maritime Sciences, Vestfold University College, P.O. Box 2243, Tønsberg, N-3103 Norway
(Dated: September 17, 2012)

Mechanically nonlinear energy harvesters driven by broadband vibrations modeled as white noise are investigated. We derive an upper bound on output power versus load resistance and show that, subject to mild restrictions that we make precise, the upper-bound performance can be obtained by a linear harvester with appropriate stiffness. Despite this, nonlinear harvesters can have implementation-related advantages. Based on the Kramers equation, we numerically obtain the output power at weak coupling for a selection of phenomenological elastic potentials and discuss their merits.

PACS numbers: 05.40.Ca, 84.60.-h, 05.45.-a, 46.65.+g

Energy harvesting from motion is a means to power wireless sensor nodes in constructions, machinery and on the human body [1, 2]. A vibration energy harvester contains a proof mass whose relative motion with respect to a frame drives a transducer that generates electrical power. Linear resonant devices are superior when driven by harmonic vibrations at their resonant frequency, but perform poorly for off-resonance conditions. As real vibrations may display a rich spectral content, sometimes of broadband nature, there has been considerable interest in using nonlinear suspensions to shape the spectrum of the harvester's response to better suit the vibrations [3–12]. The wider spectral response of nonlinear devices is expected to be beneficial for broadband vibrations.

The studies so far indicate some advantages of nonlinearities for broad-banded vibrations, but little is known about which conditions make a nonlinear harvester favorable compared to a linear one. This is due to lack of adequate theory and due to the studies being concerned about specific experimental or numerical examples of nonlinear harvesters that are compared to specific examples of linear harvesters that could have been chosen differently. Furthermore, several studies do not consider the role of electrical loading which is known to have a dramatic influence on the consequences of mechanical nonlinearities for the output power [13].

The Gaussian white noise process widely used in physics and engineering [14–17] is also important in studying broadband energy harvesting [4, 5, 13, 18–23]. It can model vibrations with a flat spectrum in the finite frequency range that the mechanical system can respond effectively to. The system itself then provides a frequency cut-off making the mathematical idealization of infinite bandwidth that characterizes white noise meaningful.

Here we investigate theoretically the behavior of mechanically nonlinear energy harvesters driven by a white noise acceleration. We derive rigorous upper bounds on the output power for arbitrary elastic potential and show that subject to mild restrictions on the device parameters, it is possible to find a linear device that performs equally well as the upper bound. We give a compact expression for the output power that we use to numerically investigate the weak coupling limit of harvesters for different quartic polynomial potentials taking electrical loading fully into account.

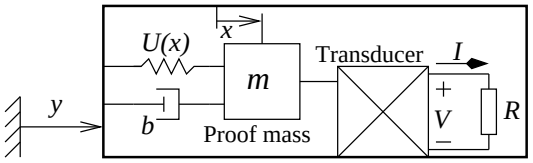

FIG. 1. Vibration energy harvester model.

An energy harvester model that isn't technology specific is shown in Fig. 1. The corresponding state space equations with a linear electromechanical transducer and a nonlinear mechanical suspension can be written

$$\dot{x} = v \tag{1}$$

$$m\dot{v} = -U'(x) - \Gamma q/C - bv + ma, \tag{2}$$

$$-R\dot{q} = RI = V = \Gamma x/C + q/C, \tag{3}$$

where m is the proof mass, x its relative displacement, v its velocity, U the open-circuit internal energy, q the transducer-electrode charge, V the output voltage, I the current, b the damping coefficient, R the load resistance, C the clamped capacitance and Γ is the transduction factor. The device-frame acceleration $\ddot{y} = -a$ is Gaussian white noise with a two-sided spectral density S_a. The equations can represent a piezoelectric or an electrostatic energy harvester. An electromagnetic harvester gives the same mathematical structure, but different physical interpretation. We use charge as the independent variable [24]. Using voltage instead is physically equivalent and also common, see e.g. [25].

Ensemble averages with respect to the stationary distribution generated by the process (1-3) will be denoted by $\langle\cdots\rangle$. The mean output power $P = \langle V^2\rangle/R$ will be our main object of interest. A number of other expressions for P immediately follow by using stationarity, (1)

and (3). We will use some of these expressions without giving the derivation.

From (3), $q = \mathcal{O}(\Gamma)$. The second term on the right hand side of (2) is $\mathcal{O}(\Gamma^2)$ and can then be dropped in the limit $\Gamma \to 0$. This is the weak coupling limit, which in the stationary state has the reduced probability density

$$W^0_{\rm st}(x,v) = \exp(-bv^2/mS_a - 2bU(x)/m^2S_a)/Z^0_{\rm st} \quad (4)$$

where $Z^0_{\rm st}$ is a normalization constant [26]. We denote expectations in this limit by $\langle\cdots\rangle_0$.

The important observation that the mean input power is $P_{\rm in} = mS_a/2$ was made in [20] where it was proved for linear harvesters. For our nonlinear system and $\Gamma = 0$, all power is dissipated in the damper, (4) implies the equipartition theorem, and $P_{\rm in} = b\langle v^2\rangle_0 = mS_a/2$. For general Γ, consider the input energy $\int_{t_1}^{t_2} mav{\rm d}t$ over a time interval. When the actually continuously differentiable a is modeled as white noise, the appropriate stochastic representation of the energy is a Stratonovich integral $mv\circ{\rm d}a$ [27]. We have $mv\circ{\rm d}a = mv{\rm d}a + mS_a{\rm d}t/2$ where $v{\rm d}a$ is an Ito integral and has zero expectation [26, 28]. The input-energy expectation is then $mS_a{\rm d}t/2$ which yields the stated expression for $P_{\rm in}$.

The observation means that $\eta = 2P/mS_a$ is an efficiency that should be maximized, as opposed to narrowband harvesting where power transfer is maximized. It also implies a power balance

$$P = mS_a/2 - b\langle v^2\rangle. \quad (5)$$

For linear harvesters, $\eta \to 1$ as $k^2Q_{\rm m} \to \infty$ where $k^2 = \Gamma^2/KC \le 1$ is the transducer electromechanical coupling factor, K is the open-circuit stiffness and Q_m is the open-circuit quality factor[13]. Hence, it is impossible to improve significantly on a linear harvester that is already very efficient. The device in [29] for example, has $k^2Q_{\rm m} \approx 7.8$ resulting in $\eta \approx 0.79$. The great number of harvesters, especially those with small volume, that perform substantially below their theoretical maximum [2], suggests that the weak coupling regime nevertheless has great practical relevance.

The load resistance determines the electrical time scale $\tau = RC$ distinguishing different regimes of operation. When τ is the fastest scale, i.e. $\tau \to 0$, we have [13]

$$P \sim \Gamma^2\langle v^2\rangle\tau/C \sim \Gamma^2\langle v^2\rangle_0\tau/C = \Gamma^2\tau mS_a/2bC. \quad (6)$$

From (3), it is readily proved that $P = \Gamma^2\tau\langle v^2\rangle/C - \tau^3\langle\dot I^2\rangle/C \le \Gamma^2\tau\langle v^2\rangle/C$. One can also show that $\langle v^2\rangle \le \langle v^2\rangle_0$. Hence, both asymptotic relations in (6) are upper bounds on the output power. We note that the bounds are valid for any U that permits a stationary distribution and that the output power is otherwise independent of U when $\tau \to 0$.

When the electrical time scale is the slowest in the system, i.e. when $\tau \to \infty$, we have [5, 13]

$$P \sim \Gamma^2\langle(x-\langle x\rangle)^2\rangle/\tau C \sim \Gamma^2\langle(x-\langle x\rangle_0)^2\rangle_0/\tau C. \quad (7)$$

The leftmost asymptotic formula in (7) is also an upper bound. This is seen by using (3) to find

$$P = \Gamma^2\langle(x-\langle x\rangle)^2\rangle/\tau C - \langle(q-\langle q\rangle)^2\rangle/\tau C \quad (8)$$

which gives the inequality when dropping the second term. The rightmost asymptotic formula in (7) need not be an upper bound as can be inferred already from linear theory. We note that (7), in contrast to (6), is strongly dependent on U as it is proportional to $\langle(x-\langle x\rangle)^2\rangle$.

The maximum power as a function of τ must necessarily be found at an intermediate value of τ between the small-τ and large-τ regimes. Since the output power is respectively insensitive and sensitive to the nature of U in these two regimes, the degree to which the maximum power can be improved by mechanical nonlinearities is an open question.

We first address the issue by deriving improved power bounds and comparing to linear behavior. Define $z = q - \langle q\rangle - D(x-\langle x\rangle) - Bv$ and find the values of the constants B and D that minimize $\langle z^2\rangle$. Eliminate covariances between x and q using $\Gamma\langle xq\rangle + \langle q^2\rangle = 0$ and use $P = \Gamma\langle qv\rangle/C$ and (8) to write the minimum value as

$$\langle z^2\rangle = \frac{\tau C}{\Gamma^2}\frac{\langle(q-\langle q\rangle)^2\rangle}{\langle(x-\langle x\rangle)^2\rangle}P - \frac{C^2P^2}{\Gamma^2\langle v^2\rangle}. \quad (9)$$

Next, use this to eliminate the variance of q in (8) and rearrange to obtain $P = (1-\langle z^2\rangle/\tau CP)P_{\rm u1} \le P_{\rm u1}$ where

$$P_{\rm u1} = \frac{\Gamma^2}{C}\frac{\tau\langle v^2\rangle\langle(x-\langle x\rangle)^2\rangle}{\langle(x-\langle x\rangle)^2\rangle + \tau^2\langle v^2\rangle}. \quad (10)$$

We see that (10) agrees with (6) and (7) in their respective limits and is a tighter bound.

The rms frequency $\omega_{\rm m} = \sqrt{\langle v^2\rangle/\langle(x-\langle x\rangle)^2\rangle}$ can be used to eliminate the displacement variance in (10). Using $P = mS_a/2 - b\langle v^2\rangle \le P_{\rm u1}$ we find a *lower* bound on $\langle v^2\rangle$ which we substitute back into the power balance equation to obtain $P \le P_{\rm u2}$ where the new bound is

$$P_{\rm u2} = \frac{mS_a}{2}\frac{\Gamma^2\tau/Cb}{1+\Gamma^2\tau/Cb+\omega_{\rm m}^2\tau^2}. \quad (11)$$

$P_{\rm u2}$ is manifestly less than $P_{\rm in}$ and is asymptotically approaching the exact result at the extreme limits of τ.

The most optimistic estimate of output power permitted by (11) is found for load resistances such that $\omega_{\rm m}\tau = 1$ and is $P_{\rm u2,Opt} = (mS_a\Gamma^2/2Cb)/(2\omega_{\rm m} + \Gamma^2/Cb)$. The exact output power of an optimally loaded linear harvester is $P_{\rm Lin,Opt} = (mS_a\Gamma^2/2Cb)/(2\omega_0 + b/m + \Gamma^2/Cb)$ where ω_0 is the open circuit resonance. The two can be made equal by choosing $\omega_0 = \omega_m - b/2m$. The stability criterion $k^2 < 1$ dictates that such a linear device is realizable if $\omega_{\rm m} > b/2m + |\Gamma|/\sqrt{mC}$, i.e. unless we have very high damping. *Therefore nonlinear harvesters are not fundamentally better than linear ones when driven by noise.*

We now consider how to directly calculate the output power. From (1) and (3) it follows that $V = (\Gamma/C)\int_{-\infty}^{t}\exp(-(t-t_1)/\tau)v(t_1)\mathrm{d}t_1$. Inserting this expression into $P = \Gamma\langle v(t)V(t)\rangle$, we obtain

$$P = \frac{\Gamma^2}{C}\int_0^\infty e^{-t/\tau}\langle v(t)v(0)\rangle \mathrm{d}t = \frac{\Gamma^2}{C}\tilde{K}_{vv}(1/\tau), \quad (12)$$

i.e. that the output power is proportional to the Laplace transform $\tilde{K}_{vv}$ of the velocity autocorrelation function.

In the weak coupling limit $\Gamma \to 0$, we can approximate $\tilde{K}_{vv}$ by its value $\tilde{K}^0_{vv}$ for $\Gamma = 0$ to obtain the leading order. $\tilde{K}^0_{vv}$ can be found from the transition probability by solving the Fokker-Planck equation corresponding to (1) and (2) with $\Gamma = 0$, i.e. the Kramers equation [30].

Without pursuing it further, we remark that an alternative method to calculate the output power, and therefore also $\tilde{K}^0_{vv}$, would be to find a *stationary* solution of the Fokker-Planck equation for the energy harvester[13] in the weak coupling limit and use $P \sim \Gamma\langle qv\rangle_0/C$ or $P \sim \Gamma\langle vV\rangle_0$.

We determine $\tilde{K}^0_{vv}$ numerically from the Kramers equation by orthogonal function expansions and matrix continued fraction methods following [30, 31]. The spatial basis functions are $\psi_n(x) = \sqrt{W(x)}\pi_n(x)$, $n = 0, 1, ...$ where $W(x) = \exp(-2bU(x)/m^2S_a)/Z_0$, Z_0 is a normalization constant and $\pi_n(x)$ are orthonormal polynomials with $W(x)$ as weight function. We express all spatial-basis matrix elements in terms of the recurrence coefficients for π_n which are determined by adapting the Lanczos method described in [32] to continuous polynomials. Dimensionless variables distinguished by asterisk subscripts and based on a characteristic length scale l_s and frequency scale ω_s are used, e.g. $P_* = P/ml_\mathrm{s}^2w_\mathrm{s}^3$, $\Gamma_* = \Gamma/\sqrt{m\omega_\mathrm{s}^2C}$, $S_{a*} = S_a/l_\mathrm{s}^2\omega_\mathrm{s}^3$ and $\tau_* = \omega_s\tau$.

We first consider the much studied symmetric quartic potential $U = Ax^2/2 + Bx^4/4$, choose l_s such that $B_* = Bl_\mathrm{s}^2/m\omega_\mathrm{s}^2 = 1$ and w_s such that $\gamma_* = b/m\omega_\mathrm{s} = 1/100$. For small values of τ_*, the output power in Fig. 2 collapses as predicted by (6) onto the same asymptotic form for both potentials. For $S_{a*} = 1.0\cdot10^{-4}$ the mass vibrates around a potential minimum, giving a performance for larger τ_* that differs between the two cases due to their different linearized stiffness. At $S_{a*} = 0.1$, the quartic term in the potential determines the behavior. In the intermediate case of $S_{a*} = 1.0\cdot10^{-3}$, the two potentials give comparable maximum power even though there is a considerable difference between them for large τ_*.

The upper bound (11) deviates significantly from the actual performance for the bi-stable potential at small S_{a*} when the longest time scale is that of interwell transitions as given by Kramers' rate problem [5, 14]. This demonstrates the necessity of the more complicated treatment, such as the numerical method used here, in predicting maximum power as opposed to bounding it.

Fig. 3 shows the output power versus the parameter $A_* = A/m\omega_\mathrm{s}^2$ when the load is optimized for every A_*. The value of the optimal τ_* in the inset varies correspondingly. The maximum power is obtained for a negative value of A_*, i.e with a bi-stable potential, like demonstrated for a fixed load in [4]. But, as the bound shows, more power can be obtained for a linear device with $\omega_0 = \omega_\mathrm{m}$. Also linear devices with the same stiffness as the nonlinear devices have at their potential minima can give more power. Therefore the motivation for utilizing nonlinear stiffness in noise harvesting is rather one of necessity than one of advantage. Implementation con-

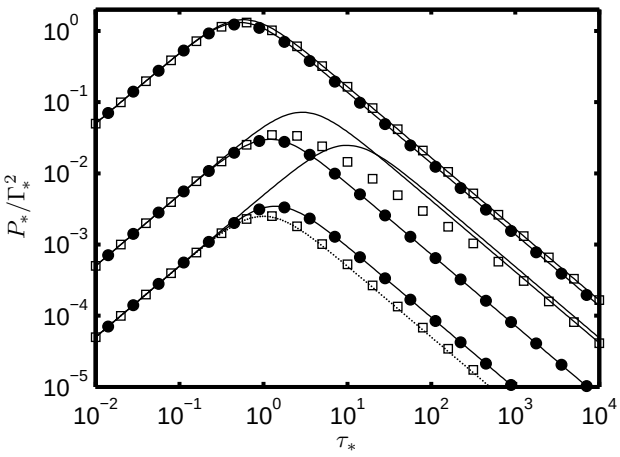

FIG. 2. Output power P_* versus electrical time scale τ_* for mono- and bistable potentials at weak coupling, $\gamma_* = 0.01$, $S_{a*} = 10^{-4}, 10^{-3}, 0.1$ (bottom to top) and $B_* = 1$. Open squares: Numerical solution for $A_* = -0.5$. Solid circles: Numerical solution for $A_* = 0.5$. Solid lines: Corresponding upper bounds. Dotted line: Solution from linearization around potential minima.

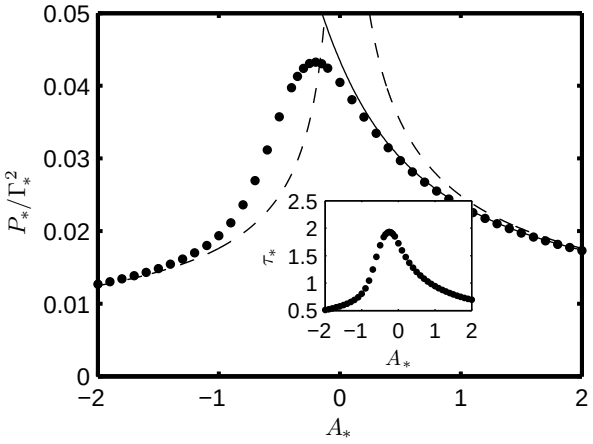

FIG. 3. Maximum output power P_* as a function of A_* at weak coupling, $\gamma_* = 0.01$, $B_* = 1$ and $S_{a*} = 10^{-3}$. Solid circles: Numerical solution. Dashed lines: Solution from linearization around potential minima. Thin solid line: upper bound. Inset shows corresponding optimal load given by τ_*.

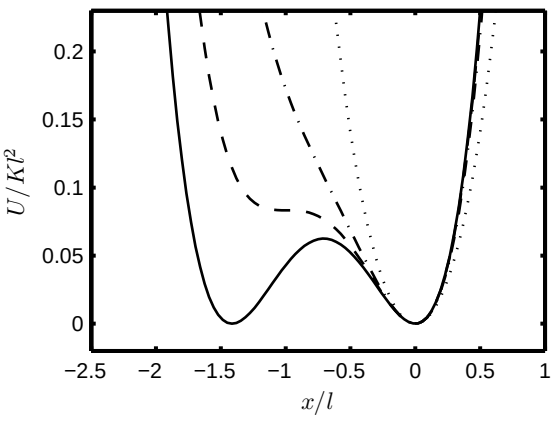

FIG. 4. Quartic potentials. Dotted line: $\xi = 0$, hardening Duffing spring; Dashed-dotted line: $\xi = \sqrt{2/3}$, negative tangential stiffness arises; Dashed line: $\xi = 2\sqrt{2}/3$, bi-stability arises; $\xi = 1$ symmetric bistable potential.

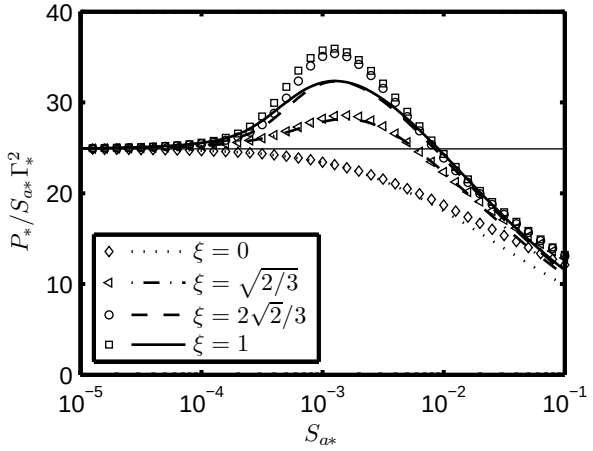

FIG. 5. Output power P_* relative to acceleration spectral density S_{a*} versus S_{a*} both for $\tau_* = 1$ (lines) and for optimal τ_* at each point (markers). Thin solid line: Linear device. $\gamma_* = 0.01$.

straints such as, e.g., package size and/or beam dimensioning may prohibit linear operation. In this respect, we can think of the quartic term of the potential as a model of proof mass confinement or beam stretching at large amplitudes.

We now consider a suspension made of a stable elastic material without built-in stress, choose $U(0) = 0$ and require $U'(0) = 0$, $U''(0) > 0$ and $U(x) > 0$ $\forall x \neq 0$. The lowest order nontrivial polynomial form can then be parametrized as

$$U(x) = \frac{1}{2}Kx^2 + \frac{K\xi}{\sqrt{2}l}x^3 + \frac{K}{4l^2}x^4 \qquad (13)$$

where $|\xi| < 1$ and l is a length scale, see Fig. 4. We choose $\omega_s = \sqrt{K/m}$ and $l_s = l$ as characteristic scales. A linear system with stiffness constrained to the same value K as in (13) is used for comparison.

Fig. 5 shows that the nonlinear devices with $\xi \neq 0$ give an S_{a*}-range of better performance than their linear counterpart. This is the case even with $\tau_* = 1$ which is optimal only for the linear device. The consistently lower power for $\xi = 0$ is due to the stiffening nature of the potential which shifts the spectrum to higher frequencies. The other potentials have a range of softening behavior causing a shift to lower frequencies and higher power. The velocity spectral densities in Fig. 6 demonstrate this shift for the bistable potential with $\xi = 1$ and the monostable potential with $\xi = 2\sqrt{2}/3$. Despite their differences, these two potentials give very similar performance and spectral shape. Note that comparing instead to a linear system with $\omega_0 = 0.5\omega_s$, which is within the $S_{a*} = 1 \cdot 10^{-3}$-responses in Fig. 6, would give $P_*/S_{a*}\Gamma_*^2 \approx 50$ outperforming all cases in Fig. 5. Even though we only considered simple phenomenological potentials (13), the broadening and flattening of the spectrum and the initial better-than-linear power-

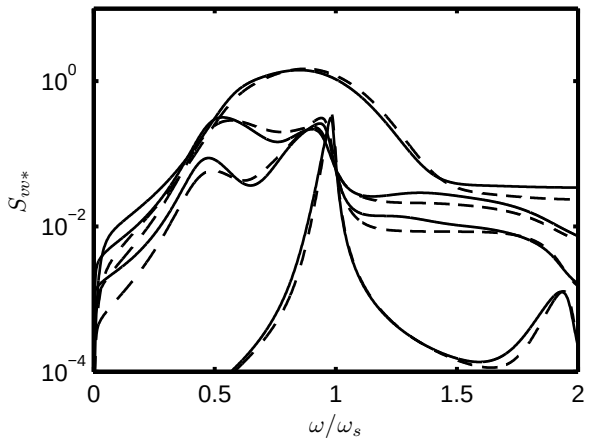

FIG. 6. Velocity spectral density versus frequency at weak coupling for $S_{a*} = 1 \cdot 10^{-4}, 5 \cdot 10^{-4}, 1 \cdot 10^{-3}, 5 \cdot 10^{-3}$. Solid lines: $\xi = 1$. Dashed lines: $\xi = 2\sqrt{2}/3$.

characteristic replicate experiments on a device with an asymmetric monostable potential [11].

We have shown that when driven by white noise, harvesters with nonlinear stiffness do not have the fundamental performance advantage over linear ones that one could have expected from their wider spectrum. This followed for efficient devices from considerations on input power and for general coupling from power bounds. Numerical examples were given for weak coupling. The findings do not preclude advantages of nonlinear-stiffness harvesters subject to vibrations significantly different from wide band noise, e.g. off-resonance, sufficiently band-limited vibrations. Implementation constraints may render a nonlinear stiffness unavoidable or a desired value of linear stiffness unattainable. We demonstrated advantages when linear stiffness was constrained.

I thank Prof. J.T. Scruggs for useful correspondence. This work was funded by The Research Council of Norway under grant no. 191282.

* E-mail: Einar.Halvorsen@hive.no

[1] S. P. Beeby, M. J. Tudor, and N. M. White, Meas. Sci. Technol. **17**, R175 (2006).

[2] P. D. Mitcheson, E. M. Yeatman, G. K. Rao, A. S. Holmes, and T. C. Green, Proc. IEEE **96**, 1457 (2008).

[3] S. Burrow and L. Clare, in *2007 IEEE International Electric Machines Drives Conference, IEMDC '07*, Vol. 1 (Antalya, Turkey, 2007) pp. 715–720.

[4] F. Cottone, H. Vocca, and L. Gammaitoni, Phys. Rev. Lett. **102**, 080601 (2009).

[5] L. Gammaitoni, I. Neri, and H. Vocca, Appl. Phys. Lett. **94**, 164102 (2009).

[6] A. Erturk, J. Hoffmann, and D. J. Inman, Appl. Phys. Lett. **94**, 254102 (2009).

[7] M. S. M. Soliman, E. M. Abdel-Rahman, E. F. El-Saadany, and R. R. Mansour, J. Micromech. Microeng. **18**, 115021 (11pp) (2008).

[8] S. C. Stanton, C. C. McGehee, and B. P. Mann, Appl. Phys. Lett. **95**, 174103 (2009).

[9] M. Marzencki, M. Defosseux, and S. Basrour, J. Microelectromech. Syst. **18**, 1444 (2009).

[10] B. Marinkovic and H. Koser, Appl. Phys. Lett. **94**, 103505 (2009).

[11] D. S. Nguyen, E. Halvorsen, G. U. Jensen, and A. Vogl, J. Micromech. Microeng. **20**, 125009 (2010).

[12] S. D. Nguyen and E. Halvorsen, J. Microelectromech. Syst. **20**, 1225 (2011).

[13] E. Halvorsen, J. Microelectromech. Syst. **17**, 1061 (2008).

[14] N. G. van Kampen, *Stochastic processes in physics and chemistry* (Elsevier, Amsterdam, 2007).

[15] R. W. Clough and J. Penzien, *Dynamics of structures*, 2nd ed. (McGraw-Hill, New York, 1993).

[16] S. Haykin, *Communication Systems*, 2nd ed. (John Wiley & Sons, Inc., New York, 1983).

[17] K. J. Åström, *Introduction to stochastic control theory* (Academic Press, New York, 1970).

[18] H. A. Sodano, D. J. Inman, and G. Park, J. Intel. Mat. Syst. Str. **16**, 67 (2005).

[19] E. Lefeuvre, A. Badel, C. Richard, D. Guyomar, and L. Petit, in *Symposium on Design, Test, Integration and Packaging of MEMS/MOEMS–DTIP'06* (Stresa, Lago Maggiore, Italy, 2006) arXiv:0711.3309v1.

[20] J. Scruggs, J. Sound Vibr. **320**, 707 (2009).

[21] L. G. W. Tvedt, D. S. Nguyen, and E. Halvorsen, J. Microelectromech. Syst. **19**, 305 (2010).

[22] M. F. Daqaq, J. Sound Vibr. **329**, 3621 (2010).

[23] S. F. Ali, S. Adhikari, M. I. Friswell, and S. Narayanan, J. Appl. Phys. **109**, 074904 (2011).

[24] H. A. C. Tilmans, J. Micromech. Microeng. **6**, 157 (1996).

[25] D. Guyomar, A. Badel, E. Lefeuvre, and C. Richard, IEEE Trans. Ultrason., Ferroelectr., Freq. Control **52**, 584 (2005).

[26] C. W. Gardiner, *Handbook of Stochastic Methods*, 3rd ed. (Springer-Verlag, Berlin-Heidelberg, 2004).

[27] B. Øksendal, *Stochastic Differential Equations* (Springe-Verlag, Berlin, Heidelberg, 2007).

[28] H.-H. Ko, *Introduction to Stochastic Integration* (Springer Science+Business Media, Inc., New York, 2006).

[29] F. Goldschmidtboeing, M. Wischke, C. Eichhorn, and P. Woias, J. Micromech. Microeng. **21**, 045006 (2011).

[30] H. Risken, *The Fokker–Planck Equation: Methods of Solutions and Applications*, 2nd ed., Springer series in synergetics, Vol. 18 (Springer-Verlag, New York, 1996).

[31] K. Voigtländer and H. Risken, J. Stat. Phys. **40**, 397 (1985).

[32] W. Gautschi, J. Comput. Appl. Math. **178**, 215 (2005).